Progress In Electromagnetics Research Letters, Vol. 102, 19–26, 2022

Bandpass Filter Design with Stub-Loaded Uniform Impedance Resonator and L-Shaped Feed Structure

Yun Xiu Wang*, Wei Chao Yang, and Min Jiang

Abstract—Microstrip single-band and dual-band bandpass filters (BPFs) are presented in this paper. Firstly, a pair of open-ended stubs of less than $\lambda/4$ in length is connected to a uniform impedance resonator (UIR) at two symmetrical positions with respect to its centre, and at the same time other two open-circuited stubs with different lengths are loaded in the middle of the resonator. By virtue of parallel-coupling structure at I/O ports, a single-band BPF is constructed centered at 2.2 GHz with 10.6% 3-dB bandwidth, and two transmission zeros are implemented at the right side of the passband. Next, the L-shaped I/O coupled lines are applied to suppress the inherent spurious response of the stub-loaded resonator. As a result, a dual-band BPF with two passbands at 2.2 GHz and 5.2 GHz, which is self-contained with three transmission zeros between the two passbands, is constituted. Finally, the proposed bandpass filters are designed and fabricated to provide an experimental validation for the predicted performances.

1. INTRODUCTION

Bandpass filters (BPFs) are essential instruments in modem communication systems, which can pass desired signals but prevent unwanted ones. Due to the increasing shortage of spectrum resources, sharpened rejection skirts in close proximity to the passband are the fundamental requirement in filter design. So far, various techniques have been proposed to produce transmission zeros (TZs). These TZs can be located near the cut-off frequencies so as to improve selectivity. On the other hand, they can also be used to increase their stopband characteristics. Firstly, cross coupling technique was first proposed to produce TZs by Pierce in [1], and until 1965 it was implemented with a three cavity waveguide filter in [2]. There are many kinds of cross coupling structures. Among them, the cascaded triplet (CT)/Cascaded Quadruplet (CQ) topology [3–6] can independently realize one or two TZs, which are independent of resonators. These structures are easy to debug and facilitate large-scale production. Based on the traditional non-adjacent resonators cross-coupled filters, the source/load (S/L) coupling is further proposed. It can generate up to N TZs, which was first proposed by Bell [7, 8]. Since then, many filter design schemes using S/L coupling technology have gradually appeared. A BPF was designed in [9] by using the mutual coupling of stepped impedance hairpin resonators, supplemented with a split-ring defected ground structure, and two TZs on the lower stopband were introduced to improve the selectivity. At the same time, referring to the source-load coupling technique in [10], the authors introduced a TZ on the right side of the passband. Another important way to generate TZs is to let the signal pass through two different paths which have similar magnitudes and nearly have a phase deference of $(2n+1)\pi$, and as a result, they will be canceled out each other at some frequencies so as to introduce TZs. In [11], a BPF with two TZs was realized by integrating a shunt inductor and a gap-coupled capacitor. Similarly, in [12], multiple TZs were generated due to nearly $(2n+1)\pi$ phase difference of path I and path II. In addition, microstrip transmission lines with stubs loaded can also

Received 9 November 2021, Accepted 20 December 2021, Scheduled 2 January 2022
* Corresponding author: Yun Xiu Wang (109wyx@163.com).
The authors are with the School of Electronic and Information Engineering, China West Normal University, Nanchong 637009, China.

generate TZs at some specified frequencies, so they are often used to design filters. A simple dual-mode dual-band BPF with asymmetrical TZs was presented in [13], which applied stubs-loaded UIRs. Another paper [14] proposed a compact BPF using multi-mode stub-loaded resonator. The resonator was loaded with a short ended stub in the center along with four pairs of open-ended stubs.

Dual-band filters are often formed by combining two different filters with sharing common input and output coupled-feed lines [15, 16]. Although these dual-band filters are more flexibly designed, they also suffer from large area and difficult debugging. Tri-band BPFs using two stub-loaded dual mode resonators and two intra-coupled internal resonators were reported in [18] and [19] where multiple TZs were generated so as to ensure that the designed filters had good selectivity. However, the authors did not give the reasons for the TZs. In [20], a pair of asymmetrical step impedance resonators was applied to realize a dual band filter, then a half wavelength UIR was added below the transmission line to achieve a triple band response. The coupling between these resonators and the input/output ports bring out five TZs.

In this paper, a single-band and a dual-band BPFs are presented by using a stubs-loaded resonator. New L-shaped feed lines are applied to suppress the unwanted second spurious frequency. Therefore, a dual-band BPF with two passbands operated at 2.2 GHz and 5.2 GHz is constituted. Predicted frequency responses are finally verified via measurement of the fabricated prototype filters on a substrate with a thickness of 1.27 mm and dielectric constant of 10.8.

2. THEORETICAL ANALYSIS

As shown in Figure 1, the proposed resonator can be considered as configured by loading a pair of open-ended stubs, denoted by length l_1 and width W_1, at two symmetrical positions with respect to a $\lambda_g/2$ UIR. Other two open-circuited stubs with different lengths l_2 and l_3, and width W_1 are added in the middle of the UIR. Thus, a nonuniform transmission line resonator is formed.

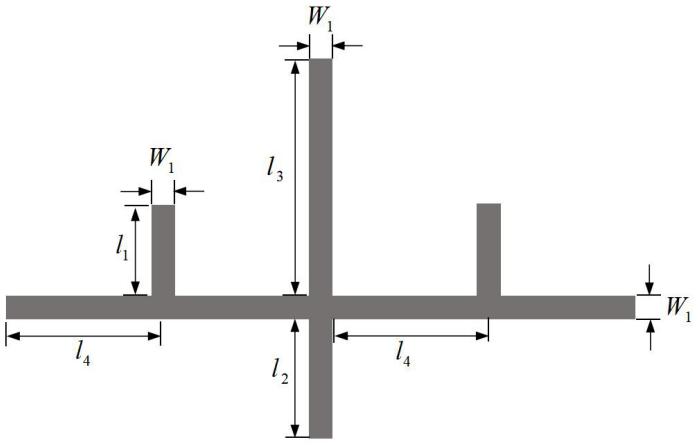

Figure 1. Non-uniform transmission line resonator.

In Figure 2, a short length of high-impedance (Z_c) lossless line is represented by a π-equivalent circuit. For a propagation constant $\beta = 2\pi/\lambda_g$ of the short line, the circuit parameters are given by [17]

$$x = \omega L' = Z_c \sin\left(\frac{2\pi}{\lambda_g} l'\right) \quad \text{and} \quad \frac{B}{2} = \omega C' = \frac{1}{Z_c} \tan\left(\frac{\pi}{\lambda_g} l'\right) \tag{1}$$

which can be obtained by equating the $ABCD$ parameters of the two circuits, here λ_g is the guided wavelength, and Z_c is the characteristic impedance.

At the open end of a stub with a width of W_1, the fields do not stop abruptly but extend slightly further because of the effect of fringing field. This effect can be modeled with an equivalent shunt capacitance C_i or with an equivalent length of transmission line l_i, as shown in Figure 3. The relation

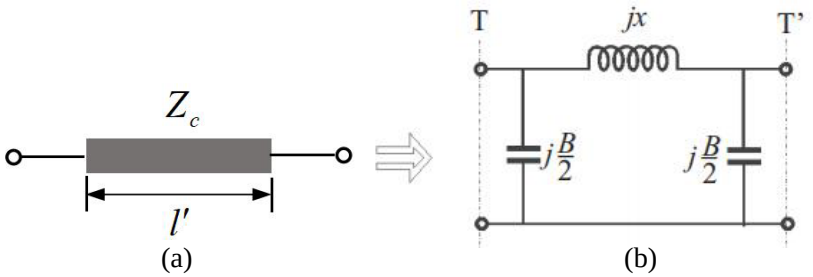

Figure 2. High-impedance short-line element.

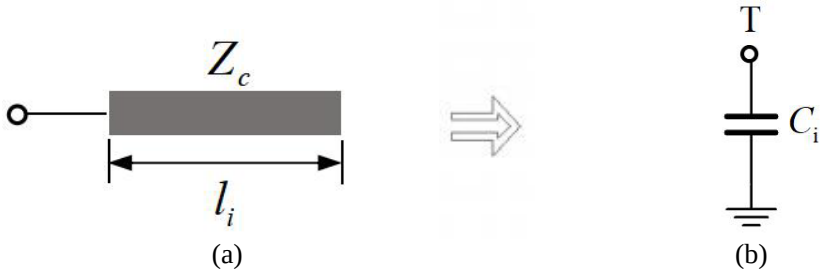

Figure 3. Stub element.

between the two equivalent parameters may be found by [17]

$$l_i = \frac{cZ_cC_i}{\sqrt{\varepsilon_{re}}} \tag{2}$$

c is the light speed in vacuum, and ε_{re} is the effective relative permittivity.

On the basis of Figure 2 and Figure 3, the equivalent circuit of Figure 1 can be represented by Figure 4 when the resonator is loosely coupled with I/O ports by $C = 0.01$ pF. The structural dimensions of the resonator can be obtained from Eqs. (1) and (2). To investigate the characteristic of the resonator, it is analyzed by ADS on a substrate with a thickness of 1.27 mm and a dielectric constant of 10.8. Figure 5 exhibits the amplitude of S_{21} for the equivalent circuit when C' and L' are set to 0.2 pF and 3.27 nH, respectively. It can be observed from Figure 5 that an additional TZ appears. It stems from the added stubs at the symmetrical position. Moreover, the TZ tends to shift from 4.1 GHz to 3.6 GHz and 3.2 GHz as C_1 increases from 1.2 pF to 1.4 pF and 1.6 pF under $C_2 = 2.1$ pF, $C_3 = 2.8$ pF, corresponding to l_1 which rises from 7 mm to 8 mm and 9 mm when l_2 and l_3 are fixed to 12 mm and 16 mm in Figure 1 according to formulas (1) and (2).

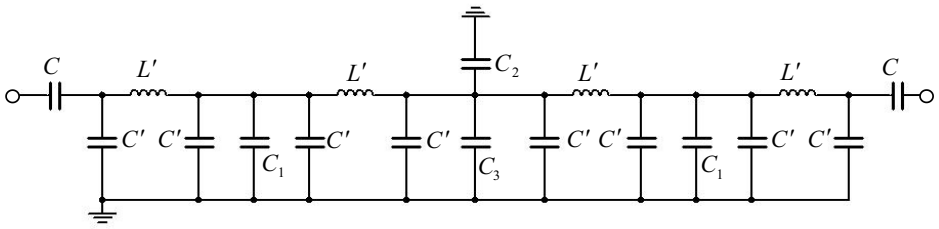

Figure 4. Lumped-parameter equivalent circuit of Figure 1.

Figure 6 plots the simulated $|S_{21}|$ of equivalent circuit of Figure 4 with different lengths l_2 and l_3. The third mode location, shown in Figure 6(a), is basically pushed up as l_2 decreases from 12 mm to 11 mm and 10 mm when $l_1 = 8$ mm and $l_3 = 16$ mm are kept unchanged. Similarly, as depicted in Figure 6(b), the first mode now tends to shift to the lower frequencies as l_3 increases from 16 mm to

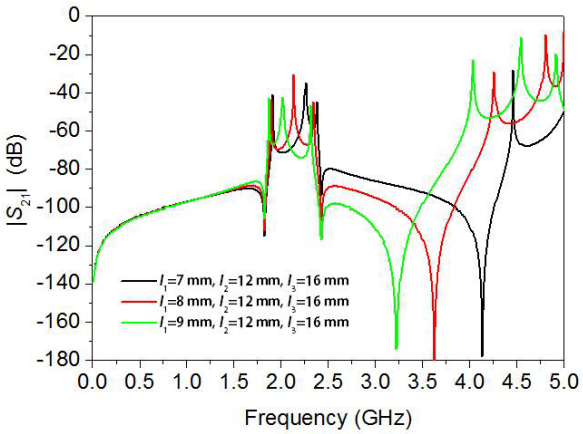

Figure 5. Simulated $|S_{21}|$ of the proposed resonator with different lengths of l_1 when l_2 and l_3 set to be 12 mm and 16 mm.

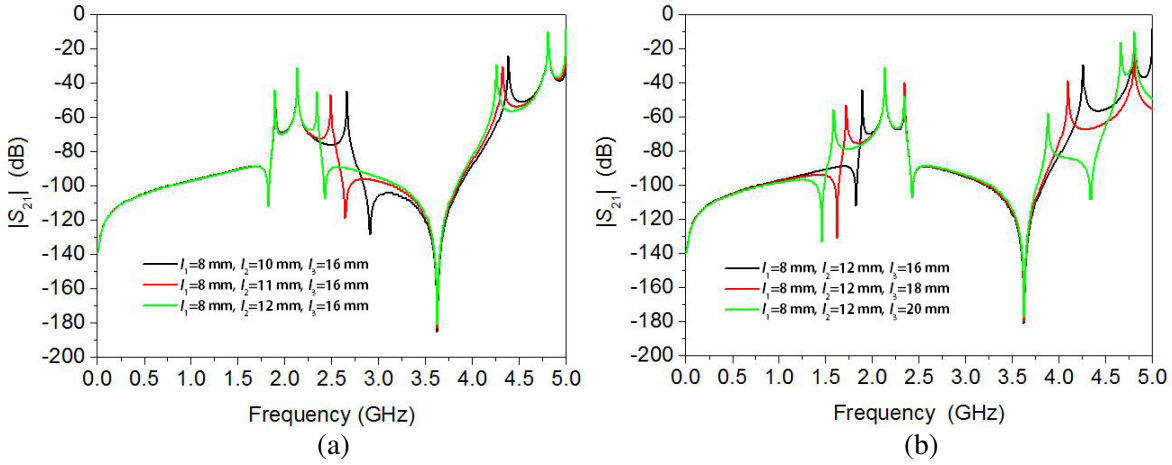

Figure 6. Simulated $|S_{21}|$. (a) Different lengths of l_2 with fixed $l_1 = 8$ mm and $l_3 = 16$ mm. (b) Different lengths of l_3 with fixed $l_1 = 8$ mm and $l_2 = 12$ mm.

18 mm and 20 mm under the fixed $l_1 = 8$ mm and $l_2 = 12$ mm. It means that we can easily adjust the bandwidth by adjusting the length of the stubs loaded in the center.

3. FILTER DESIGN AND IMPLEMENTATION

As previously mentioned, the overall length of the UIR roughly is equal to $\lambda_g/2$ at the desired center frequency. It can be estimated by

$$4l_4\,(\text{mm}) = \frac{300}{f_o\,(\text{GHz})\sqrt{\varepsilon_{re}}} \tag{3}$$

By introducing two parallel-coupled-lines at the two sides of the resonator in Figure 1, a BPF is constructed, and the layout with detailed dimensions is illustrated in Figure 7(a).

Figure 7(b) shows the simulated and measured results. The simulation is carried out by ADS. The two sets of results show good agreement with each other. A slight deviation may be due to the unexpected tolerance in fabrication, SMA connectors and inaccurate substrate characterization. The passband centered at 2.2 GHz is achieved with a fractional bandwidth of 8.6%, showing that the measured maximal in-band insertion loss is 2.1 dB, and minimum in-band return loss is 24.0 dB. There are two TZs at 2.35 and 3.62 GHz, and a passband is located at the second harmonic frequency of

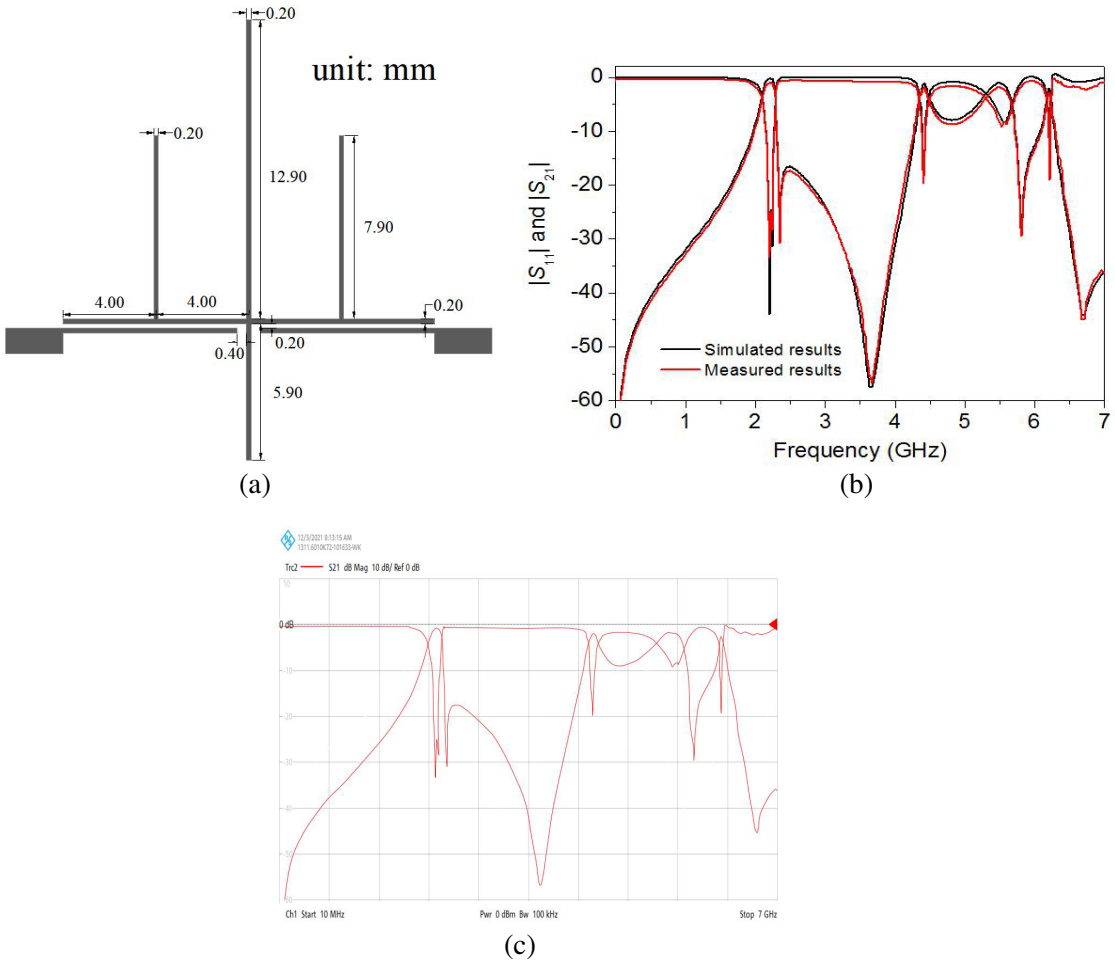

Figure 7. (a) Layout of the proposed single-pass-band BPF. (b) Comparison between simulated and measured results. (c) The snapshot and measurement setup exported from R&S VNA.

Figure 8. L-folded coupled-line section.

4.4 GHz. Figure 7(c) shows the snapshot and measurement setup exported from ROHDE&SCHWARZ ZNB40 vector network analyzer (R&S VNA). In order to realize dual-band response with second harmonic suppression, an L-type coupled line structure is applied, shown as in Figure 8. This L-type coupled line is utilized to realize two-paths external coupling and thereby generate additional TZs. Meanwhile, it can also be used to shift the position of the second harmonic passband so as to realize dual passbands. Figure 9(a) shows the simulated and measured responses of this L-type coupled lines dual-band BPF when all dimensions of the resonator are kept unchanged, and only the value of $l = 2$ mm is gradually tuned so that the additional TZ can be adjusted to the desired frequency location. Then, the dual-band BPF, embedded in Figure 9(a), is fabricated. Figure 9(b) is the snapshot and measurement

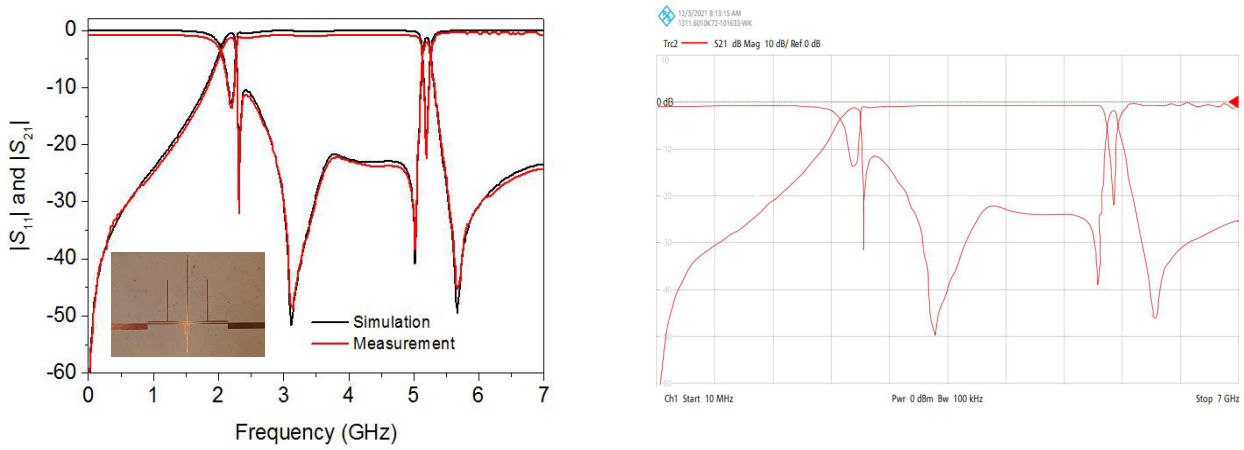

Figure 9. (a) Simulated and measured responses with the photograph of the fabricated dual-band BPF. (b) The snapshot and measurement setup exported from R&S VNA.

setup exported from R&S VNA.

The measured insertion/return losses at 2.2 and 5.2 GHz are 1.31/2.34 dB and 13.5/22.2 dB. As described above, two finite TZs appear at 2.3 and 3.1 GHz at the right side of the 1st passband mainly due to the added stubs. For the 2nd passband, a pair of finite TZs can also be produced at 5.0 and 5.7 GHz via cross coupling, and these two TZs are attributed to the out-of-phase signal interference between the mainline coupling path and cross couplings, so as to get the high rejection skirts. The three TZs between the two passbands ensure that the dual-band has excellent passband-to-passband isolation characteristic. The overall circuit area excluding two feeding ports is 16.0 mm × 19.1 mm, $0.39\lambda_g \times 0.46\lambda_g$, where λ_g is the guided wavelengths at $f_0^{\mathrm{I}} = 2.2$ GHz. Finally, the comparisons between the proposed dual-band BPF and other typical dual-band BPFs are shown in Table 1. It can be seen that the presented one has the maximum TZs and good out-of-band rejection. Moreover, the design method and structure are simple, which is suitable for engineering application.

Table 1. Performance comparison with other reported dual-band BPFs.

Reference	Center frequency (GHz)	S_{21} (dB)	Number of TZs	Size ($\lambda_g \times \lambda_g$)
[13]	1.8/2.4	1.02/1.2	1	0.21 × 0.51
[15]	1.8/2.4	1.0/1.1	3	0.20 × 0.23
[16]	2.34/5.18	1.37/1.23	3	0.30 × 0.33
This work	2.2/5.2	1.31/2.34	4	0.39 × 0.46

4. CONCLUSION

In this letter, a simple and effective design method for single-band and dual-band filter has been presented. Firstly, a single-band BPF is designed by introducing a stubs-loaded resonator. After detailed optimal design, measured results of the fabricated filter have exhibited excellent passband performances. But unfortunately, there exist spurious passband at twice the center frequency. Thus, we propose an L-type coupling line in I/O ports. This coupling structure produces additional TZs to ensure good isolation between the two passbands, and meanwhile one pair of TZs at both sides of the second passband improves the passband selectivity performance. On the other hand, it also moves the position of the second harmonic to 5.2 GHz. Measured results of the fabricated filters have exhibited excellent performances as described in the analysis.

ACKNOWLEDGMENT

This work is supported in part by the Meritocracy Research Funds of China West Normal University under Grant 17YC054, Key projects of Sichuan Education Department under Grant 16ZA0172, and Study Abroad and Return Fund of China West Normal University under Grant 15B001.

REFERENCES

1. Pierce, J. R., "Coupling of modes of propagation," *Journal of Applied Physics*, Vol. 25, No. 2, 179–183, 1954.
2. Kurzrok, R. M., "General three-resonator filters in waveguide," *IEEE Trans. Microw. Theory Techn.*, Vol. 14, No. 1, 46–47, 1966.
3. Cameron, R. J. and J. D. Rhodes, "Asymmetric realizations for dual-mode bandpass filters," *IEEE Trans. Microw. Theory Techn.*, Vol. 29, No. 1, 51–58, 1981.
4. Levy, R., "Direct synthesis of cascaded quadruplet (CQ) filters," *IEEE Trans. Microw. Theory Tech.*, Vol. 43, No. 8, 2940–2945, 1995.
5. Franti, L. F. and G. M. Paganuzzi, "Odd-degree pseudoelliptical phase-equalized filter with asymmetric band-pass behaviour," *IEEE European Microwave Conference*, 111–116, 1981.
6. Hong, J. S. and M. J. Lancaster, "Microstrip triangular patch resonator filters," *IEEE MTT-S International Microwave Symposium Digest*, 331–334, 2000.
7. Bell, H. C., "Canonical lowpass prototype network for symmetric coupled-resonator bandpass filters," *Electronics Letters*, Vol. 10, No. 13, 265–266, 1974.
8. Bell, H. C., "Canonical asymetric coupled-resonator filters," *IEEE Trans. Microw. Theory Tech.*, Vol. 30, No. 9, 1335–1340, 1982.
9. Zhang, M., M. Li, P.-J. Zhang, K. Duan, B. Jin, L. Huang, and Y. Song, "A novel miniaturized bandpass filter basing on stepped-impedance resonator," *Progress In Electromagnetics Research Letters*, Vol. 97, 77–85, 2021.
10. Ieu, W., D. Zhou, D. Zhang, et al., "Compact dual-mode dual-band HMSIW bandpass filters using source-load coupling with multiple transmission zeros," *Electronics Letters*, Vol. 55, No. 4, 210–222, 2019.
11. Wang, C.-H., Y.-S. Lin, and C. H. Chen, "Novel inductance-incorporated microstrip coupled-line bandpass filters with two attenuation poles," *IEEE MTT-S Int. Microw. Symp. Dig.*, Vol. 3, 1979–1982, 2004.
12. Wang, L. T., Y. Xiong, W.-J. Wang, L. Gong, Z. Li, X. Q. Li, and Z.-L. Liang, "Design of compact transversal wideband bandpass filter with wide upper stopband," *Progress In Electromagnetics Research M*, Vol. 96, 79–87, 2020.
13. Wattikornsirikul, N. and M. Kumngern, "Dual-mode dual-band bandpass filter with asymmetrical transmission zeros," *Progress In Electromagnetics Research M*, Vol. 86, 193–202, 2019.
14. Sami, A. and M. Rahman, "A very compact quintuple band bandpass filter using multimode stub loaded resonator," *Progress In Electromagnetics Research C*, Vol. 93, 211–222, 2019.
15. Konpang, J. and N. Wattikornsirikul, "Dual-mode dual-band bandpass filter with high cutoff rejection by using asymmetrical transmission zeros technique," *Progress In Electromagnetics Research M*, Vol. 100, 225–236, 2021.
16. Wang, Y. X., Y. L. Chen, W. H. Zou, W. C. Yang, and J. Zen, "Dual-band bandpass filter design using stub-loaded hairpin resonator and meandering uniform impedance resonator," *Progress In Electromagnetics Research Letters*, Vol. 95, 147–153, 2021.
17. Hong, J.-S. and M. J. Lancaster, *Microstrip Filter for RF/Microwave Application*, Wiley, New York, 2001.
18. Rahman, M. and J.-D. Park, "A compact tri-band bandpass filter using two stub-loaded dual mode resonators," *Progress In Electromagnetics Research M*, Vol. 64, 201–209, 2018.

19. Rahman, M. U., D.-S. Ko, and J. D. Park, "A compact tri-band bandpass filter utilizing double mode resonator with 6 transmission zeros," *Microwave and Optical Technology Letters*, Vol. 60, No. 7, 1767–1771, 2018.
20. Basit, A., M. Irfan Khattak, J. Nebhen, A. Jan, and G. Ahmad, "Investigation of external quality factor and coupling coefficient for a novel SIR based microstrip tri-band bandpass filter," *PLoS ONE*, Vol. 16, No. 10, e0258386, 2021.